Desalination and Water Treatment
www.deswater.com

doi: 10.5004/dwt.2023.29391

287 (2023) 182–190
March

Adsorption characteristic of Cd^{2+} on the nano-hydroxyapatite/biochar hybrid materials derived from rice husk and eggshells

Zhuang Zhang[a,b], Shuqin Zhang[a,b,*], Dajun Ren[a,b], Xiaoqing Zhang[a,b], Kan Tang[a,b], Xu Zhang[a,b]

[a]*College of Resources and Environmental Engineering, Wuhan University of Science and Technology, Hubei, China, Tel.: +86 15327311490; emails: zhangshuqin@wust.edu.cn (S. Zhang), 752204928@qq.com (Z. Zhang), dj_ren@163.com (D. Ren), zhangxiaoqing@wust.edu.cn (X. Zhang), 794724143@qq.com (K. Tang), 3212148544@qq.com (X. Zhang)*
[b]*Hubei Key Laboratory for Efficient Utilization and Agglomeration of Metallurgic Mineral Resources, Wuhan University of Science and Technology, Wuhan, China*

Received 13 October 2022; Accepted 11 February 2023

ABSTRACT

Industrial wastewater of cadmium ions in the environment needs to be solved urgently. Nano-hydroxyapatite and low-cost rice husk-egg shells biochar were successfully hybridized to form nano-hydroxyapatite/biochar hybrid materials (HBC) for the adsorption of Cd^{2+} in aqueous solution. Scanning electron microscopy, BET, X-ray diffraction and Fourier-transform infrared spectroscopy were used to characterize HBC. The results showed that compared with the biochar (BC), the adsorption efficiency and adsorption capacity of HBC were greatly improved. Specifically, the adsorption efficiency was increased by 50%, and the saturated adsorption capacity was increased from 23.835 to 35.2875 mg/g, which was increased by 48%. The adsorption mechanism of HBC on Cd^{2+} is complex. Chemical adsorption and multilayer adsorption provide the most important contribution, and various adsorption methods such as surface complexation, ion exchange, dissolution and precipitation also affect the adsorption of Cd^{2+}. In general, HBC is an efficient and environmentally friendly adsorbent, which can be used for the removal of Cd^{2+} from aqueous solution and has high adsorption capacity and cost effectiveness.

Keywords: Biomass; Biochar; Nano-hydroxyapatite; Cd^{2+}; Adsorption

1. Introduction

Over the past decades, with rapid industrialisation and urbanisation, water pollution by heavy metals has become one of the most important environmental concerns worldwide due to the bioaccumulative and toxic nature [1]. Unlike most organic pollutants, even very low concentrations of heavy metals in the environment can have direct or indirect adverse effects on animals, plants and humans [2]. Heavy metals such as cadmium are common in wastewater from manufacturing and mining activities. Long-term exposure or ingestion of cadmium may lead to serious disease problems such as liver and kidney damage [3], osteomalacia [4], reproductive system disorders [5], damage to the human immune system [6]and cancer [7]. When untreated cadmium wastewater enters the water and soil, it is absorbed by aquatic animals or plants and can be further enriched in the human body through the food chain. Therefore, the effective removal of cadmium from wastewater is an urgent problem.

At present, various techniques have been studied and applied to remove cadmium from water. The commonly used methods are chemical precipitation [8], reverse osmosis [9], membrane filtration techniques [10], adsorption [11],

* Corresponding author.

ion exchange [12], and electrokinetic repair [13]. Among them, adsorption is considered as a promising method due to its cost-effectiveness, high treatment efficiency and simple operation [14], so the search for an efficient, economical and green adsorbent is a hot topic of current research. Many types of adsorbents such as activated carbon [15], biochar [16,17], agricultural waste [18], biomass [19], clay [20], zeolite [21] and natural or synthetic polymers [22] have been widely used for the adsorption of heavy metals such as cadmium. Although traditional adsorbent materials such as graphene, activated carbon and carbon nanotubes have shown good results in removing pollutants from aqueous solutions, their expensive processing and regeneration costs have prevented their large-scale application [23,24]. It is the focus of current adsorbent research to find low-cost and high-efficiency adsorbent raw materials.

Biochar, made from biomass heated and decomposed under anoxic or anaerobic conditions, has received much attention because of its simple preparation process, wide source of raw materials, better adsorption of heavy metals, low production cost, and being environmentally friendly [25]. The production cost of biochar is estimated to be about 3%–6% of the cost of commercial carbon-based adsorbents [26]. This has led to biochar being extensively studied in recent years. Although biochar has many advantages in the adsorption of heavy metals, it also has defects such as poor selectivity and low adsorption capacity in the adsorption of heavy metals. Therefore, in order to make biochar better used in wastewater treatment, there have been many studies on the functionalization of biochar by nanomaterials [27,28]. Considering the effectiveness and economics of heavy metal removal, the use of hydroxyapatite hybrid biochar is a suitable choice.

Hydroxyapatite (HAP) is a green and highly efficient mineral [29], which has a special crystal structure with strong binding power for divalent heavy metal ions. In addition, it is an environmentally friendly material that is less likely to cause secondary pollution to the environment, especially nano-hydroxyapatite (nHAP), a new functional material for the treatment of environmental pollution [30], which has a stronger adsorption capacity for heavy metals due to its smaller particle size and larger specific surface area. However, there are two main problems in using nano-hydroxyapatite as adsorbent. Firstly, the chemicals required in the preparation of nano-hydroxyapatite may cause environmental pollution. Second, nano-hydroxyapatite can agglomerate in water, resulting in a significant reduction in the surface area of the nano-hydroxyapatite, which reduces the adsorption capacity of the target pollutant [31]. Therefore, the preparation of nano-hydroxyapatite from natural materials is the key to solving the first problem. Although nano-hydroxyapatite can be extracted from animal bones such as bovine or fish bones, problems continue to arise due to the variability of the physical and chemical properties of the raw material [32]. 7.2 million tons of eggshell waste were produced annually worldwide [33]and eggshells contain 94% calcium carbonate, 1% magnesium carbonate, 1% calcium phosphate, and 4% organic matter [34]. If these waste eggshells are allowed to be turned into treasure, not only is it waste reuse, but it is also a way to reduce the environmental pollution caused by waste eggshells. Using waste eggshells as one of the raw materials for the preparation of hydroxyapatite would not only reduce manufacturing costs but also reduce the environmental pollution from waste eggshells. For the second problem, the porous structure of biochar can be used to prevent the aggregation of nano-hydroxyapatite, which can ensure its adsorption capacity. In addition, the biochar In addition, biochar materials can improve their adsorption capacity and adsorption selectivity by nano-hydroxyapatite hybridization.

Therefore, in this paper, we hybridized low-cost biochar and hydroxyapatite from rice husk and eggshell for the adsorption removal of Cd^{2+}. The adsorption kinetics, adsorption isotherms, and adsorption mechanism of biochar hybrid materials (HBC) on Cd^{2+} were studied.

2. Materials and methods

2.1. Chemical reagents

$Cd(NO_3)_2{\cdot}4H_2O$, NaOH, HNO_3, NH_3H_2O, KH_2PO_3, and C_2H_5OH were all analytical reagent grade and purchased from Sinopharm Chemical Reagent Co., Ltd., China; All solutions in this experiment were diluted using ultrapure water (resistivity > 18.2 MU/cm).

2.2. Preparation of material

The rice huck was washed with the ultrapure water, dried, ground and sieved through 100 mesh. Rice husk powder was transported into the tube furnace (Tian Jin Zhong Huan Electric Furnace Co., Ltd., SK-G05123k, China) and heated from room temperature to 550°C at a rate of 5°C/min in a nitrogen atmosphere and continuous pyrolysis at this temperature for 120 min. After cooling to room temperature, the material was removed and stored under dry conditions. The adsorbent produced by the above method was named biochar. Eggshells collected from canteens were treated according to previous methods [35,36]. The eggshell powder was transported into the tube furnace and heated from room temperature to 550°C at a rate of 10°C/min in a nitrogen atmosphere and continuous pyrolysis at this temperature for 120 min. After that, the eggshell powder was continuously pyrolyzed from 450°C to 900°C in a nitrogen atmosphere for 240 min. After cooling to room temperature, the material was removed under dry conditions.

The HBC was prepared as follows. According to the previous research [37], a constant amount of treated eggshells was weighed into ultrapure water, and the pH was adjusted to acidic and completely dissolved in the sonication device. Then a certain amount of biochar (BC) was weighed and put into the solution, and suspension A was obtained after stirring for 6 h. The potassium dihydrogen phosphate solution was slowly poured into solution A. The pH of the final solution was adjusted to 10, aged for 24 h, filtered and washed to neutral, and dried. Finally, the obtained product was placed in the tube furnace and heated from room temperature to 600°C at a heating rate of 10°C/min in a nitrogen atmosphere where it was continuously pyrolyzed for 120 min. After cooling to room temperature, the material was removed and stored under dry conditions. The adsorbent produced by the above method was named HBC.

2.3. Characterization of biochar

The surface morphology of the samples before and after modification was characterized by scanning electron microscopy (SEM), (Tescan, MiraLms, Czech Republic), and the change in crystal shape before and after modification was characterized by X-ray diffraction (XRD; Rigaku, SmartLab SE, Japan). Moreover, the change in functional groups before and after reaction was characterized by Fourier-transform infrared spectroscopy (FTIR) (Thermo Fisher Scientific, IS50, USA). The characteristics of the specific surface area and pore structure are measured by fully automatic specific surface and porosity analyzer (ASAP 2020, PLUS HD88, Micromeritics, USA).

2.4. Adsorption experiment

1.3909 g $Cd(NO_3)_2$ $4H_2O$ was weighed in a 1 L volumetric flask and diluted with ultrapure water to 500 mg/L stock solution. All experiments were carried out at 25°C ± 1°C. 0.04 g of HBC and 40 mL Cd^{2+} solution were added into a 100 mL conical flask. It was shaken on a thermostatic oscillator at the condition of 160 rpm. After the adsorption process, the adsorbent was separated by a 0.45 μm syringe filter, and the residue was measured by a flame atomic absorption spectrophotometer (Jena AG, novaa 350, Germany). Except for isothermal adsorption, the concentrations of Cd^{2+} solution in other adsorption experiments were all 50 mg/L. In addition to the study of dosage factors, in other adsorption experiments, 0.04 g HBC was placed in a conical flask.

The adsorption kinetics were performed over 720 min (5, 10, 20, 30, 60, 90, 120, 180, 240, 300, 360, 480, and 720). The adsorption isotherm experiments were established with Cd^{2+} concentrations of 50 ~ 500 mg/L (50, 100, 200, 300, 400, and 500) after 360 min oscillation. The isotherms were obtained after the pH influence experiment, dosage influence experiment, and adsorption kinetics. In all adsorption experiments, three groups of parallel experiments were set.

2.5. Analysis methods

The adsorption capacity and removal percentage of Cd^{2+} by the adsorbent were calculated according to Eqs. (1) and (2):

$$q_t = \frac{\left(C_0 - C_t\right)V}{m} \tag{1}$$

$$\eta = \frac{\left(C_0 - C_t\right)}{C_0} \times 100\% \tag{2}$$

where q_t is the amount of Cd^{2+} adsorbed at the time of adsorption t (mg/g); V is the volume of the solution (L); η is the removal percentage of Cd^{2+}; m is the mass of biochar (g); C_0 is the initial concentration of Cd^{2+} (mg/L); C_e is the equilibrium concentration of Cd^{2+} (mg/L).

2.6. Adsorption model

Adsorption kinetic model: pseudo-first-order and pseudo-second-order models and the Weber–Morris kinetic model were used to fit the adsorption experimental data. The specific equations were as follows, where the pseudo-first-order kinetic model equation was as Eq. (3), the pseudo-second-order kinetic model equation was as Eq. (4), and the Weber–Morris kinetic model equation was as Eq. (5).

$$q_t = q_e\left[1 - \exp\left(-k_1 t\right)\right] \tag{3}$$

$$\frac{t}{q_t} = \frac{1}{k_2 q_e^2} + \frac{t}{q_e} \tag{4}$$

$$q_t = k_{ip} t^{0.5} + C \tag{5}$$

where q_m is the equilibrium adsorption capacity (mg/g); k_1 is the rate constant of the pseudo-first-order kinetic model (min^{-1}); k_2 is the rate constant of the pseudo-second-order kinetic model (g/mg·min); k_{ip} is the diffusion rate constant within the particle ($mg/g \cdot min^{1/2}$); t is the adsorption time (min).

Isothermal adsorption model: Langmuir model and Freundlich model were used to fit and analyze the data. The equations were as follows, where the Langmuir model equation was as Eq. (6), and the Freundlich model equation was as Eq. (7).

$$q_e = \frac{q_m K_L C_e}{1 + K_L C_e} \tag{6}$$

$$q_e = K_F C_e^{1/n} \tag{7}$$

where q_e is the equilibrium adsorption capacity (mg/g); q_m is the saturated adsorption capacity (mg/g); C_e is the concentration of Cd^{2+} when the adsorption reaches equilibrium (mg/L); K_L is the Langmuir adsorption coefficient; K_F is the Freundlich adsorption coefficient.

3. Results and discussion

3.1. Characterization

In order to study the morphology and microstructure between BC and HBC, SEM was used for characterization. It can be seen from Fig. 1A and B that BC has a porous structure, which is beneficial to the adsorption of heavy metals by BC. It can be seen from Fig. 1C and D that nHAP has covered the surface and pore structure of biochar, indicating that the hybridization effect is obvious.

The XRD patterns of BC and HBC can be seen in Fig. 2A. According to the standard powder diffraction file (09-0432), the characteristic peaks (002), (211), (300), (202), (310) and (222) of HAP appeared on the HBC pattern, indicating that nHAP has been loaded onto rice husk biochar [38] and also proving that the surface of BC on SEM is indeed covered by nHAP. Fig. 2B shows the FTIR of HBC before and after the adsorption of Cd^{2+}. The 3,409.5 cm^{-1} represents the bending mode of hydroxyl groups in water, 472.5, 565.5, 602, 1,035 and 1,089 cm^{-1} corresponds to the vibration of phosphate groups, and 1,419 and 454 cm^{-1} corresponds to carbonate groups, indicating the presence of carbonate [39], which

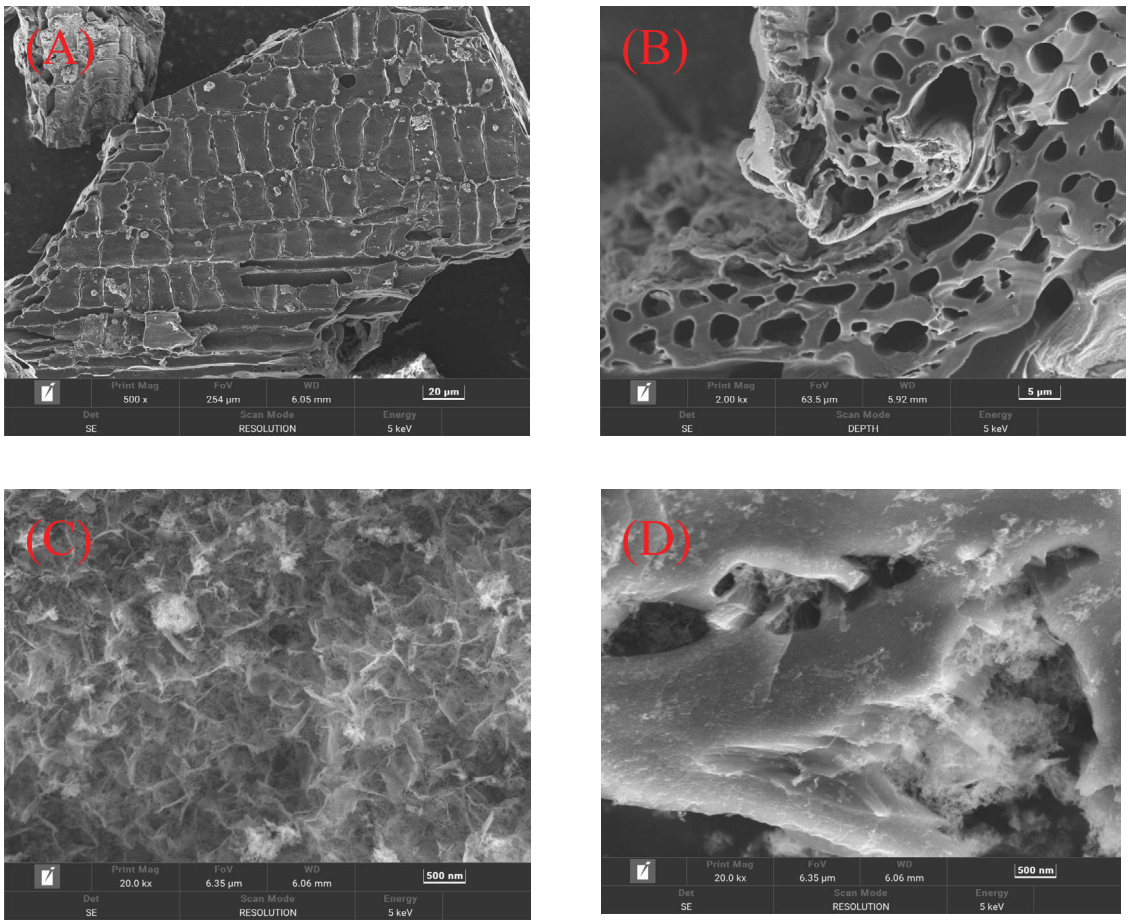

Fig. 1. Scanning electron microscopy images of the biochar (A and B) and HBC (C and D) at different expansion ratios.

may come from biochar and the changes in the peaks before and after the adsorption of Cd^{2+} indicated that $–PO_4$ and $–CO_3$ participated in the adsorption process.

The nitrogen adsorption–desorption isotherms of HBC are shown in Fig. 2C. According to the nitrogen adsorption isotherms of IUPAC, it shows type II and type IV with H3 hysteresis loops. The high adsorption ($P/P_0 < 0.2$) at low relative pressure indicates the presence of microporous structure in HBC (type II). HBC shows H3 type hysteresis loops between P/P_0 = 0.25–1.0, possibly including mesoporous structures such as nHAP nanoparticle plate slit structure, cracks structure, and wedges structure [40], which is consistent with the SEM results. The BET specific surface area of HBC is 70.3028 m^2/g, the pore size was 14.6694 nm, and the total pore volume was 0.266614 cm^3/g. The pore size distribution of HBC can be seen in Fig. 2D. The pore structure of HBC is mainly distributed in the mesopore range, and the larger pore size is beneficial to the diffusion of macromolecular heavy metal ions in the HBC voids.

3.2. Effect of pH and dosage on the adsorption of Cd^{2+}

According to other literature, solution pH has a significant effect on the adsorption of heavy metal ions [41,42], mainly reflected in two aspects. Firstly, the hydrogen ions in the acidic solution will protonate the active site, which will prevent the metal ions from approaching. Secondly, the alkaline solution containing a large amount of hydroxide ions will cause the precipitation of Cd^{2+}, which may interfere with the actual adsorption amount of Cd^{2+}. Therefore, the pH range of this experiment was 2~6. According to Fig. 3A, it can be seen that the adsorption effect of HBC on Cd^{2+} in pH 2~6 environments. When pH < 3, HBC had almost no adsorption effect on Cd^{2+}. With the increase of pH, the adsorption efficiency of HBC for Cd^{2+} increased. The reason is that when pH < 3, the nHAP in HBC is dissolved [43] [Eq. (8)], resulting in the destruction of the crystal structure of nHAP, thereby inhibiting the adsorption of Cd^{2+} by HBC. With the increase of pH, on the one hand, the H^+ that competes with heavy metal ions is greatly reduced, which means that the adsorption sites occupied by H^+ on HBC are decreasing, and the corresponding adsorption sites for heavy metal ions are increasing [44].

On the other hand, more OH^- enhances the electronegativity of the adsorbent surface and enhances the adsorption effect on heavy metal ions. At pH 6, the adsorption of Cd^{2+} by HBC reached equilibrium and the maximum adsorption capacity was 30.127 mg/g. In addition, between pH 2 and pH 3, the adsorption efficiency of HBC for Cd^{2+} is greatly improved, indicating that the zero point of HBC may be between pH 2 and 3. The pH value corresponding to the zero point potential is pHzpc. When pHzpc, the surface of

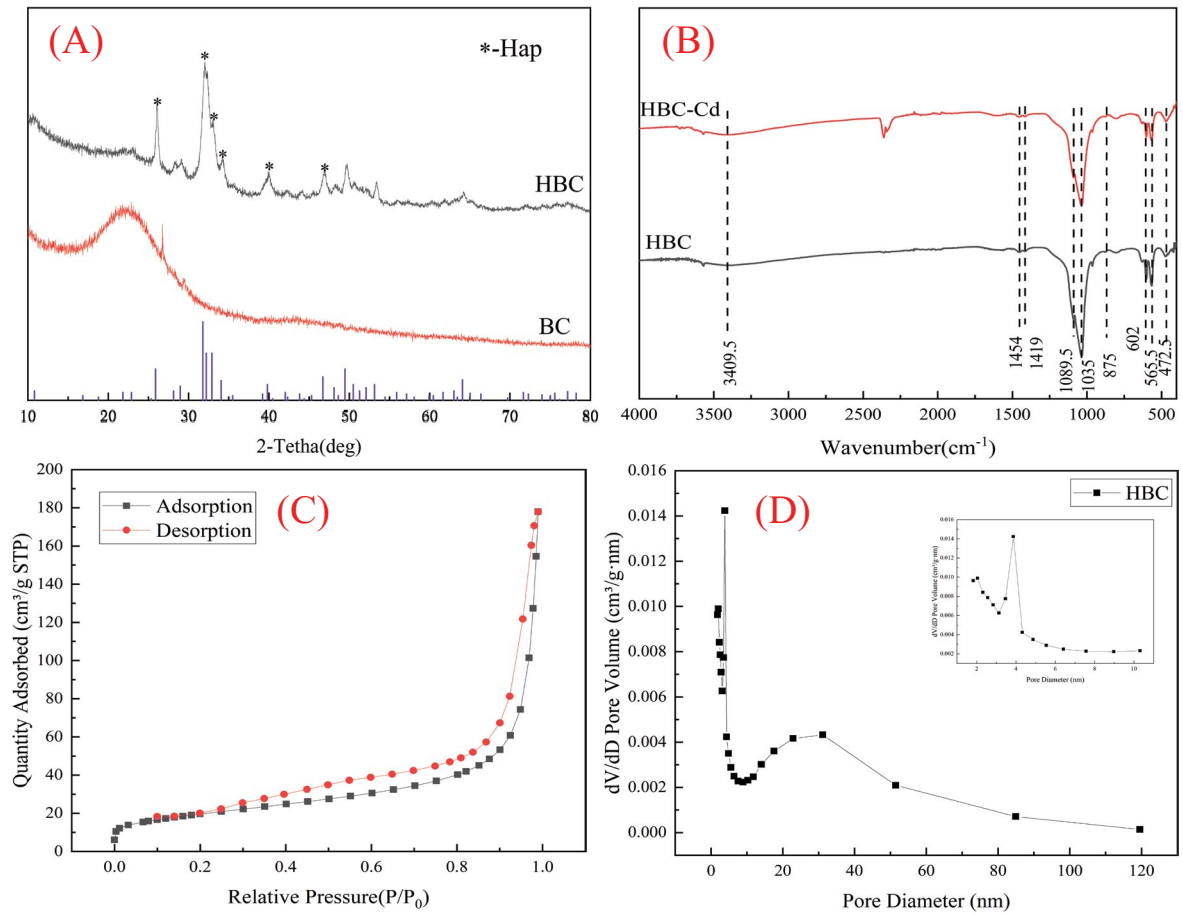

Fig. 2. X-ray diffraction patterns of biochar and HBC (A), Fourier-transform infrared spectrums of the HBC before and after sorption of Cd^{2+} (B), N_2 adsorption–desorption isotherms (C) and the pore-size distribution (D) of HBC.

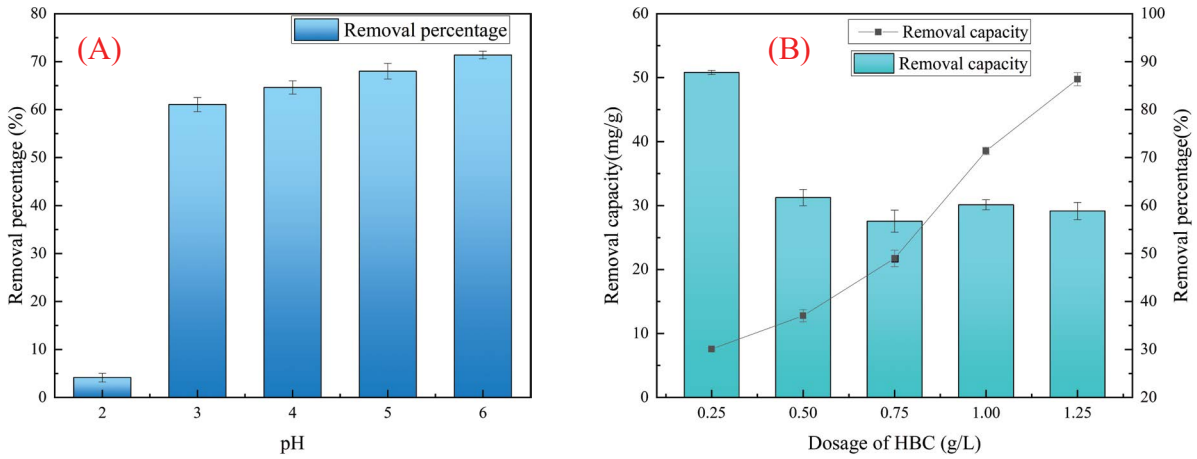

Fig. 3. Effects of pH (A) and dosage (B) on the adsorption of contaminants by HBC.

the adsorbent presents a negative potential, which produces electrostatic attraction with Cd^{2+}, thereby improving the adsorption effect [42].

$$Ca_{10}(PO_4)_6(OH)_2 + 2H^+ \rightarrow 10Ca^{2+} + 6PO_4^{3-} + 2H_2O \quad (8)$$

The relationship between HBC dosage and Cd^{2+} adsorption capacity and adsorption efficiency are shown in Fig. 3B. When the HBC dosage was gradually increased from 0 to 1.25 g/L, the adsorption efficiency continued to grow, which was due to the increasing specific surface area and available adsorption sites as the amount of HBC increased [43].

However, the adsorption capacity of Cd^{2+} was different from the adsorption rate, and the adsorption capacity was gradually reduced. This is because when the concentration and volume of Cd^{2+} are constant, with the increase of HBC dosage, the active sites are not fully utilized, and the aggregation and overlap of active sites lead to the decrease of the surface area of adsorption, which leads to the decrease of the adsorption capacity of HBC to Cd^{2+} in water. Considering the factors such as cost, adsorption efficiency, and adsorption capacity, the actual adsorbent dosage is 1 g/L.

3.3. Adsorption kinetics

Fig. 4A shows the effect of adsorption time on the adsorption of Cd^{2+} by BC and HBC. The adsorption amount of BC and HBC increased rapidly in the first 60 min, gradually increased after 60 min, and reached the adsorption equilibrium at 360 min. At each time point, the adsorption capacity of HBC for Cd^{2+} was higher than that of BC. Compared with BC, the equilibrium adsorption capacity of HBC increased from 23.85 to 35.28 mg/g, which increased by about 48%. This indicated that the adsorption effect of the HBC was better than that of the BC. The main reason for the rapid increase of adsorption capacity in the first 60 min is that when the concentration and volume of Cd^{2+} solution are constant, BC and HBC have a large number of active sites in the early stage of adsorption, the concentration of Cd^{2+} is higher in the early stage of adsorption, the mass transfer power is larger, and the concentration of Cd^{2+} in the later stage of adsorption is lower. After 60 min, the adsorption rate was lower than the initial rate, which was due to the rapid decrease of the concentration difference of Cd^{2+} and the active sites on the surface of BC and HBC were less and less. In the later stage of adsorption, with the depletion of surface active sites of BC and HBC and the weakening of intraparticle diffusion of BC and HBC, the adsorption rate decreased and the adsorption reached saturation.

In order to better characterize the adsorption mechanism of Cd^{2+} on BC and HBC, the pseudo-first-order kinetics, pseudo-second-order, and intraparticle diffusion equations were used to characterize the adsorption kinetics. The fitting results of pseudo-first-order and pseudo-second-order kinetic models are shown in Fig. 4A and Table 1. The correlation coefficient R^2 of the pseudo-second-order kinetic equation of BC and HBC was higher, so the adsorption process of Cd^{2+} by BC and HBC can be well described by the pseudo-second-order kinetic equation, indicating that the adsorption of Cd^{2+} by BC and HBC was closer to chemical adsorption. The fitting results of the intraparticle diffusion model are shown in Fig. 4B and Table 2. The adsorption fitting curve of BC can be divided into two stages. The first stage was the liquid film diffusion stage, the second-stage was the intraparticle diffusion stage, and the adsorption of BC in the intraparticle diffusion stage was basically completed. The adsorption fitting curve of HBC can be divided into three stages, which was consistent with the classical three-stage adsorption theory. The first stage was the liquid film diffusion stage, in which Cd^{2+} diffuses to the HBC surface through the liquid film. The second-stage was the intraparticle diffusion stage. Cd^{2+} further migrates from the HBC surface to the adsorption

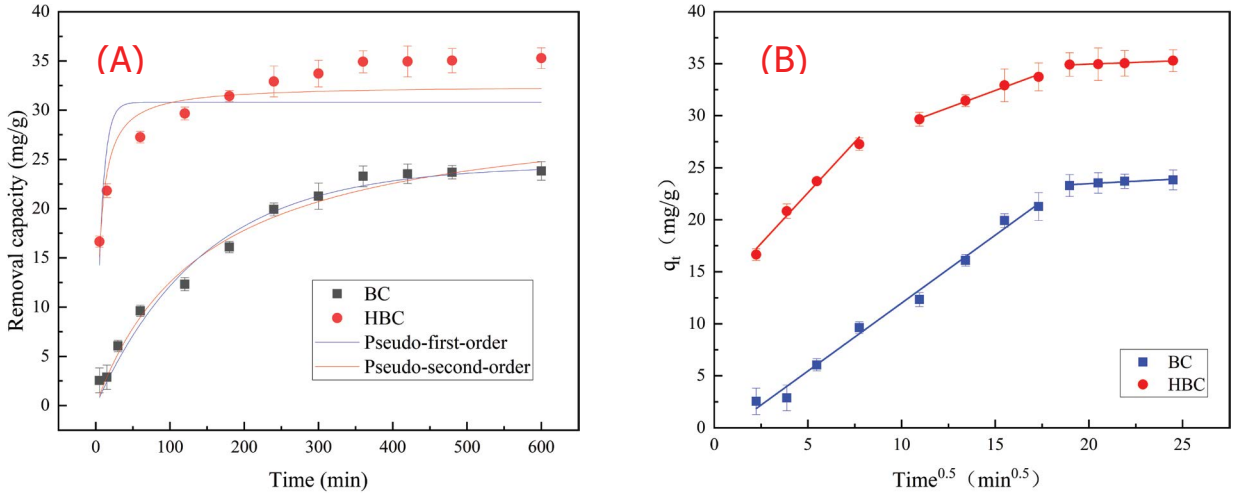

Fig. 4. Adsorption kinetics for Cd^{2+} by biochar and HBC (A) and fitting curves of Weber–Morris model (B).

Table 1
Parameters of adsorption kinetics

Adsorbent	Pseudo-first-order equation			Pseudo-second-order equation		
	q_e (mg/g)	k_1 (min^{-1})	R_1^2	q_e (mg/g)	k_2 (g/min·min)	R_2^2
BC	24.3546	0.0069	0.97265	30.79692	0.000222	0.98077
HBC	30.8023	0.12431	0.75822	32.52142	0.00532	0.90292

site, and the intraparticle diffusion played a major role in this stage. The third stage was the adsorption reaction stage, at which the adsorption reaches equilibrium. The intraparticle diffusion equation parameters of BC and HBC can be seen in Table 2. For BC, $K_{i1} > K_{i2}$, $C_1 < C_2$, the linear slope of the liquid film diffusion stage was larger than that of the intraparticle diffusion stage, indicating that the adsorption rate was faster in the liquid film diffusion stage. The C value in the intraparticle diffusion stage was larger than that in the liquid film diffusion stage, which reflected that the boundary layer resistance became larger and the adsorption rate decreased. This stage was the main step limiting the adsorption rate of BC. For HBC, $K_{i1} > K_{i2} > K_{i3}$, $C_1 < C_2 < C_3$, which indicated that HBC had the largest adsorption rate in the early stage of adsorption, mainly due to the presence of a large number of adsorption sites in the early stage of adsorption. When the outer surface of HBC reached saturation in the first stage, the adsorption on the inner surface of HBC increased, and the diffusion resistance of Cd^{2+} increased. The curve fitted by the internal diffusion equation of BC and HBC did not cross the origin, indicating that the internal diffusion of particles was not the only rate-controlling step, and the adsorption rate was also affected by reactions such as ion exchange and dissolution precipitation.

3.4. Adsorption isotherm

Cd^{2+} solutions with concentrations of 50, 100, 200, 300, 400, and 500 mg/L were taken in a 40 mL volumetric flask. The solution pH was 6, 0.04 g of HBC was added, and the solution was shaken at 25°C for 360 min. It can be seen from Fig. 5 that with the increase of solution concentration, the equilibrium adsorption capacity increases, but the increase rate decreases. This is because with the increase of initial Cd^{2+} concentration, the chance of Cd^{2+} contacting the active sites on the surface of HBC increases, which is conducive to the adsorption of Cd^{2+} by surface functional groups. However, a certain amount of adsorbent can provide a certain contact area and adsorption site. When the concentration reaches a certain level, the adsorption site has been fully utilized, and the adsorption gradually reaches saturation [47]. The maximum adsorption capacity was 124.5 mg/g. Langmuir and Freundlich isothermal adsorption models were used to fit the experimental data, and Fig. 5 is the fitting results of Langmuir equation and Freundlich equation. corresponding adsorption isotherm fitting parameters are shown in Table 3. At 25°C, the Freundlich fitting correlation coefficient was higher than that of Langmuir, and the correlation was more significant. The adsorption of Cd^{2+} by HBC was more in line with the Freundlich adsorption isotherm equation, which indicated that the adsorption of Cd^{2+} by HBC was mainly based on multi-molecular layer adsorption. However, the correlation coefficients of Langmuir and Freundlich models were both > 0.9, indicating that the adsorption mechanism of HBC on Cd^{2+} was complex, and there were many adsorption methods such as ion exchange and surface complexation.

3.5. Adsorption mechanism

According to the above characterization and experiments, the adsorption mechanism of HBC on Cd^{2+} in aqueous solution was not a single chemical adsorption or physical adsorption, but a multi-mechanism adsorption including

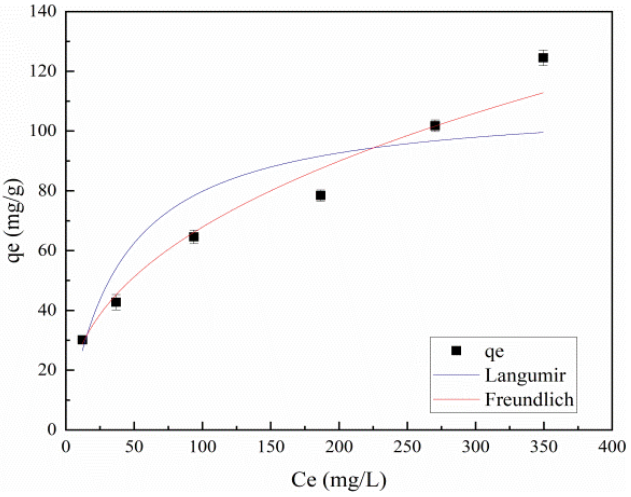

Fig. 5. Fitting curves of Langmuir and Freundlich isothermal models.

Table 2
Fitting parameters of Weber–Morris model

Adsorbent	Step 1			Step 2			Step 3		
	K_{i1} (mg/g·min$^{1/2}$)	C_1	R^2	K_{i2} (mg/g·min$^{1/2}$)	C_2	R^2	K_{i3} (mg/g·min$^{1/2}$)	C_3	R^2
BC	1.30623	–1.078	0.98577	0.09585	21.55	0.84889			
HBC	1.94832	12.84	0.97575	0.66517	22.44	0.98973	0.0685	33.58	0.9195

Table 3
Fitting parameters of isothermal adsorption models

Adsorbent	Langmuir model			Freundlich model		
	q_m	K_L	R^2	$1/n$	K_F	R^2
HBC	110.47956	38.37749	0.9065	2.46111	10.44704	0.98037

physical and chemical action. SEM and XRD results showed that nano-hydroxyapatite successfully hybridized to biochar. The pseudo-first-order and pseudo-second-order models also showed that the adsorption mechanism in the adsorption process and the diffusion in the particles were the main rate-limiting steps. FTIR results before and after adsorption indicated that the oxygen-containing functional groups (–PO_4, –CO_3) on the HBC surface adsorbed Cd^{2+} through complexation. The isothermal adsorption model further indicated that the adsorption mechanism of Cd^{2+} on HBC was complex, and Cd^{2+} underwent single-layer chemical adsorption and multi-layer physical adsorption on the surface of HBC. The experimental results of the influencing factors showed that the pH of the solution and dosage could make a great influence on the adsorption capacity and adsorption efficiency. The pH will change the surface charge of HBC, and the change of dosage will change the number of adsorption sites of HBC in water, which indicates that HBC has electrostatic interaction with Cd^{2+}. In general, the main adsorption mechanisms of Cd^{2+} on HBC are complexation, electrostatic adsorption, surface adsorption, ion exchange [Eqs. (9) and (10)], and dissolution precipitation of hydroxyapatite [Eqs. (11) and (12)].

$$10Cd^{2+} + 6PO_4^{3-} + 2H_2O \rightarrow Cd_{10}\left(PO_4\right)_6\left(OH\right)_2 + 2H^+ \quad (9)$$

$$Ca_{10}\left(PO_4\right)_6\left(OH\right)_2 + xCd^{2+} \rightarrow xCa^{2+} + Ca_{10-x}Cd_x\left(PO_4\right)_6\left(OH\right)_2 \quad (10)$$

$$Ca_{10}\left(PO_4\right)_6\left(OH\right)_2 + 14H^+ \rightarrow 10Ca^{2+} + 6H_2PO_4^- + 2H_2O \quad (11)$$

$$10Cd^{2+} + 6H_2PO_4^- + 2H_2O \rightarrow Cd_{10}\left(PO_4\right)_6\left(OH\right)_2 + 14H^+ \quad (12)$$

4. Conclusion

In this study, we successfully prepared the nano-hydroxyapatite/biochar hybrid materials (HBC). The HBC synthesized in this study exhibited superior adsorption performance for Cd^{2+}. The characterization results confirmed the successful hybridization of nano-hydroxyapatite onto biochar. The adsorption capacity of HBC was 48% higher than that of BC. The Freundlich isotherm model described the sorption well and the maximum adsorption capacity was 124.5 mg/g. Adsorption kinetics followed the pseudo-second-order model, and the Weber and Morris intraparticle diffusion model showed that the sorption mechanism included three different steps. Both physical and chemical mechanisms were involved in Cd^{2+} adsorption onto HBC. The main adsorption mechanisms were electrostatic interaction, ion exchange, and dissolution precipitation of hydroxyapatite. The results from the present study indicate that HBC could be a technically feasible and promising Cd^{2+} sorbent for wastewater treatment.

Disclosure statement

No potential conflict of interest was reported by the author(s).

Date availability statement

Due to the nature of this research, participants of this study did not agree for their data to be shared publicly, so supporting data is not available.

Acknowledgments

We are sincerely grateful to the reviewers and the editor for their useful comments that have helped us to improve the quality of our study. This work was supported by the [Wuhan Science and Technology Planning Project] under Grant [number 2020020601012274] and [Outstanding Young and Middleaged Scientific and Technological Innovation Team Plan in Hubei Province] under Grant [numberT2020002].

References

[1] P. Xu, G.M. Zeng, D.L. Huang, C.L. Feng, S. Hu, M.H. Zhao, C. Lai, Z. Wei, C. Huang, G.X. Xie, Z.F. Liu, Use of iron oxide nanomaterials in wastewater treatment: a review, Sci. Total Environ., 424 (2012) 1–10.
[2] K. Jung, S.Y. Lee, J. Choi, Y.J. Lee, A facile one-pot hydrothermal synthesis of hydroxyapatite/biochar nanocomposites: adsorption behavior and mechanisms for the removal of copper(II) from aqueous media, Chem. Eng. J., 369 (2019) 529–541.
[3] X. Wang, W. Cu, M. Wang, Y. Liang, G. Zhu, T. Jin, T. Chen, The association between life-time dietary cadmium intake from rice and chronic kidney disease, Ecotoxicol. Environ. Saf., 211 (2021) 111933, doi: 10.1016/j.ecoenv.2021.111933.
[4] Y. Ma, D. Ran, X. Shi, H. Zhao, Z, Liu, Cadmium toxicity: a role in bone cell function and teeth development, Sci. Total Environ., 769 (2021) 144646, doi: 10.1016/j.scitotenv.2020.144646.
[5] S. Ibha, S. Sinba, S. Vaibhav, Singh, R. Pratap, Impact of cadmium pollution on food safety and human health, Curr. Opin. Toxicol., 27 (2021) 1–7.
[6] D.L. Knoell, T.A. Wyatt, The adverse impact of cadmium on immune function and lung host defense, Semin. Cell Dev. Biol., 115 (2021) 70–76.
[7] J. Wu, X.M. Dong, Y.F. Zheng, J.R. Zhang, Recent research progress in molecular mechanisms of cadmium induced carcinogenesis AZN, J. Ecotoxicol., 10 (2015) 54–61.
[8] K. Tonni Agustiono, G.Y.S. Chan, L. Wai-Hung, B. Sandhya, Physico–chemical treatment techniques for wastewater laden with heavy metals, Chem. Eng. J., 118 (2006) 83–98.
[9] Y. Cui, Q.C. Ge, X.Y. Liu, T. Chung, Novel forward osmosis process to effectively remove heavy metal ions, J. Membr. Sci., 467 (2014) 188–194.
[10] Y. Zhu, J. Hu, J. Wang, Competitive adsorption of Pb(II), Cu(II) and Zn(II) onto xanthate-modified magnetic chitosan, J. Hazard. Mater., 221–222 (2012) 155–161.
[11] A.B. Perez-Marin, V.M. Zapata, J.F. Ortuno, M. Aguilar, J. Saez, M. Llorens, Removal of cadmium from aqueous solutions by adsorption onto orange waste, J. Hazard. Mater., 139 (2007) 122–131.
[12] F. Fu, Q. Wang, Removal of heavy metal ions from wastewaters: a review, J. Environ. Manage., 92 (2011) 407–418.
[13] D. Purkayastha, U. Mishra, S. Biswas, A comprehensive review on Cd(II) removal from aqueous solution, J. Water Process Eng., 92 (2014) 105–128.
[14] S. Rajput, C.U. Jr. Pittman, D. Mohan, Magnetic magnetite (Fe_3O_4) nanoparticle synthesis and applications for lead (Pb^{2+}) and chromium (Cr^{6+}) removal from water, J. Colloid Interface Sci., 468 (2016) 334–346.
[15] B. Thouraya, O. Abdelmottaleb, Improvement of oxygen-containing functional groups on olive stones activated carbon by ozone and nitric acid for heavy metals removal from aqueous phase, J. Water Process Eng., 468 (2016) 334–346.

[16] Y.C. Sun, T.T. Wang, X.Y. Sun, L. Bai, C.H. Han, P.F. Zhang, The potential of biochar and lignin-based adsorbents for wastewater treatment: comparison, mechanism, and application–a review, Ind. Crops Prod., 166 (2021) 113473, doi: 10.1016/j.indcrop.2021.113473.
[17] W.G. Yu, J.H. Li, D. Wang, Z.Y. Liang, Y.C. Zhang, The preparation of biochar from pre-oxidation of banana stem and its adsorption of Cu^{2+}, Chem. Ind. Eng. Prog., 36 (2017) 1499–1505.
[18] S.K. Gunatilake, C. Rohana, Removal of Pb(II) from contaminated water using low temperature pyrolyzed agricultural and forest waste biochars – a comparative study, Desal. Water Treat., 62 (2017) 316–324.
[19] C. Liu, C.J. Yan, S. Zhou, W. Ge, Fabrication of sponge biomass adsorbent through UV-induced surface-initiated polymerization for the adsorption of Ce(III) from wastewater, Water Sci. Technol., 75 (2017) 2755–2764.
[20] H. Li, X. Zhang, Y. Zhang, L. Jia, Y. Zhang, H. Huang, H. Ou, Y. Zhang, Adsorbent-to-photocatalyst: recycling heavy metal cadmium by natural clay mineral for visible-light-driven photocatalytic antibacterial, J. Colloid Interface Sci., 629 (2022) 1055–1065.
[21] Ž. Rudžionis, S.K. Adhikary, F.C. Manhanga, D.K. Ashish, R. Ivanauskas, G. Stelmokaitis, A.A. Navickas, Natural zeolite powder in cementitious composites and its application as heavy metal absorbents, J. Build. Eng., 43 (2021) 103085, doi: 10.1016/j.jobe.2021.103085.
[22] H.S. Ibrahim, T.S. Jamil, E.Z. Hegazy, Application of zeolite prepared from Egyptian kaolin for the removal of heavy metals: II. Isotherm models, J. Hazard. Mater., 182 (2010) 842–847.
[23] R.H. Li, J.J. Wang, Z.Q. Zhang, M.K. Awasthi, D. Du, P.F. Dang, Q. Huang, Y.C. Zhang, L. Wang, Recovery of phosphate and dissolved organic matter from aqueous solution using a novel CaO-MgO hybrid carbon composite and its feasibility in phosphorus recycling, Sci. Total Environ., 642 (2018) 526–536.
[24] H.B. Yin, M. Kong, X.H. Gu, H.U. Chen, Removal of arsenic from water by porous charred granulated attapulgite-supported hydrated iron oxide in bath and column modes, J. Cleaner Prod., 166 (2017) 88–97.
[25] R. Arpita, B. Navneeta, Efficient removal of heavy metals from artificial wastewater using biochar, Environ. Nanotechnol. Monit. Manage., 16 (2021) 100602, doi: 10.1016/j.enmm.2021.100602.
[26] J. Yoder, S. Galinato, D. Granatstein, M. Garcia-Pérez, Economic trade-off between biochar and bio-oil production via pyrolysis, Biomass Bioenergy, 35 (2011) 1851–1862.
[27] H. Samaraweera, C.U. Pittman Jr., R.V.K.G. Thirumalai, E.B. Hassan, F. Perez, T. Mlsna, Characterization of graphene/pine wood biochar hybrids: potential to remove aqueous Cu^{2+}, Environ. Res., 192 (2021) 110283, doi: 10.1016/j.envres.2020.110283.
[28] W. Wu, Z. Liu, M. Azeem, Z.Q. Guo, R.H. Li, Y.G. Li, Y.R. Peng, E.F. Ali, H.L. Wang, S.S. Wang, J. Rinkle, S.M. Shaheen, Z.Q. Zhang, Hydroxyapatite tailored hierarchical porous biochar composite immobilized Cd(II) and Pb(II) and mitigated their hazardous effects in contaminated water and soil, J. Hazard. Mater., 437 (2022) 129330, doi: 10.1016/j.jhazmat.2022.129330.
[29] K.L. Wan, L. Huang, J. Yan, B.Y. Ma, X.J. Huang, Z.X. Luo, H.G. Zhang, T.F. Xiao, Removal of fluoride from industrial wastewater by using different adsorbents: a review, Sci. Total Environ., 773 (2021) 145535, doi: 10.1016/j.scitotenv.2021.145535.
[30] T.T. Hu, L. Cang, Y.J. Wang, Y.B. Si, D.M. Zhou, Competitive adsorption kinetics of aqueous Pb^{2+} and Cu^{2+} on nano-HAP surfaces, Environ. Sci., 33 (2012) 2875–2881.
[31] Y.N. Zhu, Y.H. Jiang, Z.Q. Zhu, H. Deng, H. Ding, Y.H. Li, L.H. Zhang, J. Lin, Preparation of a porous hydroxyapatite-carbon composite with the bio-template of sugarcane top stems and its use for the Pb(II) removal, J. Cleaner Prod., 187 (2018) 650–661.
[32] G. Goller, F.N. Oktar, L.S. Ozyegin, E.S. Kayali, E. Demirkesen, Plasma-sprayed human bone-derived hydroxyapatite coatings: effective and reliable, Mater. Lett., 58 (2004) 2599–2604.
[33] Y. Feng, B. Ashok, K. Madhukar, J.M. Zhang, J. Zhang, K.O. Reddy, A.V. Rajulu, Preparation and characterization of polypropylene carbonate bio-filler (eggshell powder) composite films, Int. J. Polym. Anal. Charact., 19 (2014) 637–647.
[34] A.S.M. Bashir, Y. Manusamy, Characterization of raw eggshell powder (ESP) as a good bio-filler, J. Eng. Res. Technol., 2 (2015) 56–60.
[35] A.I. Adeogun, A.E. Ofudje, M.A. Idowu, S.O. Kareem, Facile development of nano size calcium hydroxyapatite based ceramic from eggshells: synthesis and characterization, Waste Biomass Valorization, 9 (2018) 1469–1473.
[36] D.M. Ge, F. Sun, Z. Wang, Investigation on hydroxyapatite synthesis from eggshells using hydrothermal process hydrothermal process, J. HB NORM. Univ. N Sci. Edn., 37 (2013) 60–64.
[37] Y.Y. Wang, Y.X. Liu, H.H. Lu, R.Q. Yang, S.M. Yang, Competitive adsorption of Pb(II), Cu(II), and Zn(II) ions onto hydroxyapatite-biochar nanocomposite in aqueous solutions, J. Solid State Chem., 261 (2018) 53–61.
[38] Z.M. Yang, Z.Q. Fang, L.C. Zheng, W. Cheng, P.E. Tsang, J.Z. Fang, D.Y. Zhao, Remediation of lead contaminated soil by biochar-supported nano-hydroxyapatite, Ecotoxicol. Environ. Saf., 132 (2016) 224–230.
[39] Y.Y. Xie, X.Z. Yuan, Z.B. Wu, G.M. Zeng, L.B. Jiang, X. Peng, H. Li, Adsorption behavior and mechanism of Mg/Fe layered double hydroxide with Fe_3O_4-carbon spheres on the removal of Pb(II) and Cu(II), J. Colloid Interface Sci., 536 (2019) 440–455.
[40] M. Thommes, Physisorption of gases, with special reference to the evaluation of surface area and pore size distribution (IUPAC Technical Report), Pure Appl. Chem., 87 (2015) 1051–1069.
[41] Y.Y. Wang, H.H. Lu, Y.X. Liu, S.M. Yang, Ammonium citrate-modified biochar: an adsorbent for La(III) ions from aqueous solution, Colloids Surf., A, 509 (2016) 550–563.
[42] F.J. Cao, Y. Ping, J. Zhang, H. Chen, R.J. Qu, Nanoplates of cobalt phosphonate with two-dimensional structure and its competitive adsorption of Pb(II) and Hg(II) ions from aqueous solutions, J. Ind. Eng. Chem., 20 (2014) 2568–2573.
[43] D.X. Liao, W. Zheng, X.M. Li, Q. Yang, X. Yue, L. Guo, G.M. Zeng, Removal of lead(II) from aqueous solutions using carbonate hydroxyapatite extracted from eggshell waste, J. Hazard. Mater., 177 (2010) 126–130.
[44] R. Sitko, B. Zawisza, E. Malicka, Modification of carbon nanotubes for preconcentration, separation and determination of trace-metal ions, TrAC, Trends Anal. Chem., 37 (2012) 22–31.
[45] S.T. Zhuang, Y. Liu, J.L. Wang, Covalent organic frameworks as efficient adsorbent for sulfamerazine removal from aqueous solution, J. Hazard. Mater., 383 (2020) 121126, doi: 10.1016/j.jhazmat.2019.121126.
[46] H.B. Senturk, D. Ozdes, A. Gundogdu, C. Duran, M. Soylak, Removal of phenol from aqueous solutions by adsorption onto organomodified Tirebolu bentonite: equilibrium, kinetic and thermodynamic study, J. Hazard. Mater., 172 (2009) 353–362.
[47] L.K. Zhang, Y. Wang, W.D. Wang, Y.M. Li, P. Sun, J.H. Han, Q.H. Jiang, The preparation of biochar-supported nano-hydroxyapatite and its adsorption of Pb^{2+}, Chem. Ind. Eng. Prog., 37 (2018) 3492–3501.